ADVANCED FUNCTIONAL MATERIALS
www.afm-journal.de

Unraveling Temperature-Dependent Contact Electrification between Sliding-Mode Triboelectric Pairs

Aurelia C. Wang, Binbin Zhang, Cheng Xu, Haiyang Zou, Zhiqun Lin, and Zhong Lin Wang**

The underlying mechanism on contact electrification (CE) has remained a topic of debate over centuries, and it is argued to be due to electron transfer, ion transfer, and/or even material species transfer. Recently, a previous study shows that CE is dominated by electrons, at least for solid–solid cases. Herein, by using a model detailing the charge transfer between triboelectric surfaces and thermionic emission of electrons via employing a sliding mode Ti–SiO_2 triboelectric nanogenerator (TENG), surface charge decay behavior is scrutinized in lateral-sliding mode during operation at high temperature. The temperature dependence of TENG electric output contributes to characteristic metal–dielectric and dielectric–dielectric CEs, thereby providing further evidence that electrons are the dominating transferred charges in CE. The total surface charge output of the TENG is rationalized as a direct consequence of the coupling of the rate of electron thermionic emission, the charge transfer rate of CE, and the changing rate of the contacted area between the two materials. When the contacting area is larger than the displaced area, the CE between the two materials is the major contributor to measured surface charge. Conversely, the thermionic emission of the exposed surfaces dictates when the contacting area is smaller.

1. Introduction

Efforts to establish a universal explanation of contact electrification (CE) have spanned many centuries, and yet our understanding of this commonplace phenomenon remains to be explored. Existing theories involving CE are highly material-dependent, and there lacks an agreement on an all-inclusive, dominant mechanism of CE. One primary example of this is the debate over whether the charges transferred between surfaces in metal–dielectric and dielectric–dielectric CE are electrons or ions, which has been ongoing since the early 20th century.[1] Well-established studies from the mid-20th century suggest that metal–metal CE is electron-dominated and dependent on the work function, the Volta potential difference, or the electrostatic potential difference between two metals in contact.[2] Due to charged surfaces being in a nonequilibrium state, the significant impact of contaminants, and the influence of varying length and time scales, a universal model for metal–dielectric and dielectric–dielectric CE is a challenge yet to be resolved.[3] Dielectric surface states and barrier heights have been widely accepted as entities involved in metal–dielectric charge transfer and retention, and many endeavors to theoretically characterize these processes using density functional theory measurements and electrochemical reduction reactions have been made, yet discrepancies between proposed universal models still persist.[3a,4] Recently, extensive progress has been made on this front, owing to the systematic measurement of metal–dielectric CE through real-time temperature-dependent triboelectric nanogenerator (TENG) studies, which provides a new method for exploring CE.

Nanogenerators have been one of the fastest-growing fields in energy research since their inception in 2006, and have given rise to a great deal of energy harvesting and sensing applications rooted in the Maxwell displacement current.[5] In addition to making water energy,[6] wind energy,[7] and biomechanical/ambient energy harvesting[8] for self-powered electronics with ultrahigh efficiency[9] and self-powered active sensors[5e,10] possible, TENGs have been instrumental in theoretical studies on the origin and workings of CE.[5f,11] A variety of TENG studies that suggest that electrons are the dominant CE transferred charge identity have been performed, including those based on the photoelectron emission model[12] and Kelvin force probe microscopy.[13] Moreover, a quantum mechanical model for electron transfer for dissimilar and separated atoms has been proposed.[14] Of particular note are our recent studies that demonstrated the thermionic emission of electrons and subsequent exponential decay of surface charge from the surfaces of contact–separation mode Ti–SiO_2 and Ti–Al_2O_3 TENGs at high temperatures.[15] The generation of surface charge of TENG operation was maintained until temperatures rose above 413 K, above which exponential charge decay began to be observed. The decay patterns were correlated to the electron

A. C. Wang, B. Zhang, Dr. H. Zou, Prof. Z. Lin, Prof. Z. L. Wang
School of Materials Science and Engineering
Georgia Institute of Technology
Atlanta, GA 30332-0245, USA
E-mail: zhiqun.lin@mse.gatech.edu; zhong.wang@mse.gatech.edu
Prof. C. Xu
School of Materials Science and Engineering
China University of Mining and Technology
Xuzhou 221116, China
Prof. Z. L. Wang
Beijing Institute of Nanoenergy and Nanosystems
Chinese Academy of Sciences
Beijing 100083, China
The ORCID identification number(s) for the author(s) of this article can be found under https://doi.org/10.1002/adfm.201909384.

DOI: 10.1002/adfm.201909384

thermionic emission model, suggesting electrons as the dominant charge identity in CE, and a metal–semiconductor surface states model and dielectric/metal–dielectric electron cloud–potential well model were proposed.[16] Thermionic emission is a key phenomenon in explaining the reasoning behind electron-dominated CE, and involves heating a material so that electrons gain enough thermal energy to overcome the work function and in turn, emit from the material. Few studies have been conducted on how to prevent or counteract this effect, and therefore further investigation on its involvement in high temperature TENGs is needed. An efficient TENG that consistently generates power under high temperatures has recently been developed, and indeed, the sliding mode was determined to be the best operational mode, assisted by metal supports so as to increase tight contact between triboelectric materials and quench the effects of thermionic emission.[17] The reasoning behind why the sliding mode TENG operated more efficiently at high temperatures is a pressing question in the development of related applications, and one that is furthered through this study.

Figures of merits have revealed that discrepancies between different TENG operating modes (contact–separation, sliding, freestanding triboelectric layer, single electrode contact) include their charging behavior, maximum output energy per cycle, energy conversion efficiencies, and average output power.[18] Charging behavior has been found to be different between different modes of contact in CE, including sliding, rolling, and contact–separation,[19] warranting further investigation in order to develop a more universal model of CE. There have been few studies comparing contact–separation and sliding CE in depth, but more exist that compare sliding and rolling CE due to their importance in industrial granular processes. For instance, rolling particles have been found to have less fall off of charge transfer with contact time, due to the tendency of the entire surface of a particle to come into contact through a randomized fashion, including charged and uncharged areas.[20] Discharge has been suggested as the limiting factor of contact–separation or "bouncing" particle CE as compared to continuous sliding/rolling CE. Additionally, sliding motions of cylindrical grains were found to produce less charge transfer than rolling spheres, despite spherical grains having fewer triboelectric charges on their surface than cylindrical grains due to minimization of surface area.[21] This shows that despite the saturated charge being the same for sliding and rolling friction systems,[22] the operational mode has a profound effect on overall efficiency of CE. As a vital mode of operation for TENGs in terms of versatility in energy harvesting and sensing applications, lower volume required, and uniquely efficient performance in harvesting motion, sliding mode CE is a phenomenon that begs more investigation.

Herein, we report our findings build upon our previously suggested CE mechanism by incorporating surface charge data from a sliding mode Ti–SiO_2 TENG at high temperatures. Comparisons are made against the patterns of electron emission from thermal energy of the previous contact–separation mode Ti–SiO_2 TENG, and the cause for any discrepancies and similarities is scrutinized. Finally, a modified electron cloud–potential well model for universal metal–dielectric and dielectric–dielectric CE is presented to incorporate the data from the sliding mode TENG.

2. Design and Performance of the Sliding Mode Ti–SiO_2 TENG

In order to maintain a valid comparison of our data to that from the contact–separation mode high-temperature study, a high temperature-resistant sliding variant of the previously used Ti–SiO_2 TENG was developed for this study.[15] Even though polymers are ideal materials for TENGs due to their flexible physical and chemical characteristics in exchanging charge, reducing wear, and minimizing friction, the selection of thermally stable polymers is limited in regards to our experiment.[23] Also, polymer–polymer contacts can experience intermittent motion, seizure, or stick-slip due to adhesion when tested in dry conditions.[24] This should not limit future high temperature studies to be performed on thermally stable polymers such as thermosets, since triboelectrification was found to not be directly related to friction.[22] However, friction, wear, and energy consumption of sliding materials can be affected by the presence of surface charges due to increased attractive forces between them.[25] Attracting impurities and causing wear can quickly degrade the performance of CE, and regularity of motion and minimal wear of the material should be maintained for best results.

Our testing setup was designed to support a controlled vertical sliding motion between the triboelectric pair surfaces (**Figure 1**a), which were secured on heat-resistant mica ceramic plates by clamps, with one side being a sputtered Au electrode and a SiO_2 sheet that was optionally charged using a polyurethane (PU) foam, and the other being Ti foil (Figure 1b,c). The usage of PU foam to precharge the SiO_2 surface is not only to mirror the previous contact–separation study, but to also provide enough charges for any temperature effects on these surfaces to be apparent. The addition of foam to the contact–separation study was necessary, as the room temperature output was 0.45 nC for short-circuit charge transfer Q_{SC}, indicating that the surface charges generated by contact–separation were inadequate to visualize the effects of thermionic emission.[15] The triboelectric pair of SiO_2 and Ti have low power output as TENG materials, but are heat resistant and robust, and thus fitting for this study. These surfaces were aligned and stabilized with a stainless-steel framework in a heating cabinet, and a linear motor was positioned to vertically displace the mobile SiO_2 platform from alignment with the Ti foil then return it to the starting position at an operation frequency of 0.4 Hz. The Ti–SiO_2 sliding mode TENG produced an average open-circuit voltage V_{OC} of 70 V and short-circuit current I_{SC} of 116 nA per operation cycle at room temperature (Figure S1, Supporting Information). A Cu–polytetrafluoroethylene (PTFE) TENG of the same contact area and operation frequency was fabricated for comparison, and Q_{SC} and V_{OC} were 29 nC and 70 V for the Ti–SiO_2 TENG and 94 nC and 235 V for the Cu–PTFE TENG, respectively (Figure S2, Supporting Information). Although the Ti–SiO_2 TENGs electrical output performance is less than one third that of

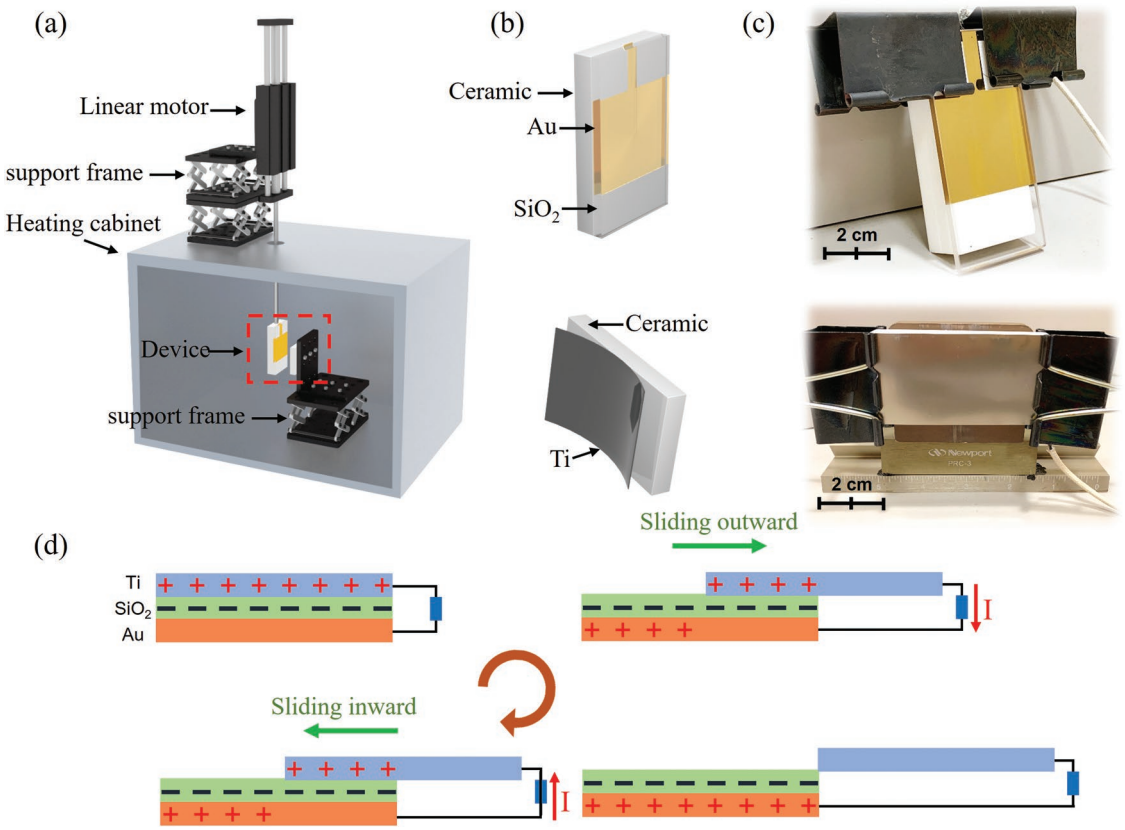

Figure 1. Setup of the high-temperature measurement platform for TENGs. a) Schematic illustration of the sliding mode Ti–SiO_2 TENG anchored with the heating cabinet and motor. b,c) Enlarged view and optical photograph of the sliding mode Ti–SiO_2 TENG within the red-dashed frame in (a). d) The working principle of the sliding mode Ti–SiO_2 TENG.

the Cu–PTFE TENG, the materials were selected for their excellent durability, stability, and comparative performance at different elevated temperatures in the preceding study.[15] Sliding CE varies between materials due to yield, deformation of surfaces, frictional heating, and material transfer, so our materials were chosen to minimize the effects of all of these.[26]

The working principle of this sliding mode Ti–SiO_2 TENG is shown in Figure 1d. As the linear motor displaces the initially aligned Ti and SiO_2 surfaces, the spontaneously generated opposite charges on both surfaces are displaced as well, creating a potential difference between the Ti foil and Au electrode. This potential imbalance drives electrons to flow from the Au electrode to the Ti foil as the surfaces are continually displaced, neutralizing the charge of the exposed area of the Ti surface. At any given point of displacement, the amount of positive charges on the Au electrode is equal to the electrons transferred to the Ti foil. The portion of Ti still in contact with SiO_2 maintains its positive charge until both surfaces are completely separated by the motion of the motor. At this point, the displacement is reversed so the Ti comes into contact with SiO_2 again, generating a spontaneous opposite charge on the area of Ti–SiO_2 contact and creating backflow of electrons to neutralize the Au electrode. The alternating current from this interchanging flow of electrons produces the electrical output of this sliding mode Ti–SiO_2 TENG.

2.1. Comparing the Sliding Mode and Contact–Separation Mode Ti–SiO_2 TENGs

The short-circuit transferred charge Q_{SC} provides a real-time quantification of the electron flow between the Ti foil and Au electrode, and a sliding mode Ti–SiO_2 TENG with ≈28 nC of initial surface charge on the SiO_2 surface shows a comparable amount of charges being transferred with each operation cycle at room temperature (**Figure 2**a). After instilling ≈28 nC of surface charge on SiO_2, Q_{SC} was monitored over time while operating at a range of temperatures, and increasingly rapid decay was observed with increasing temperature (Figure 2b). This resulted in charge decay trends similar to those found at the same temperatures in our contact–separation mode Ti–SiO_2 TENG studies,[15] albeit on much longer time scales. Through comparing the individual Q_{SC} over time plots in Figure 2c–h from the sliding mode TENG measurements to those at the same temperatures from the contact–separation mode TENG study, we find that thermionic emission of electrons is less efficient at depleting Q_{SC} to below 1 nC and surface charges are retained for longer periods of time for sliding mode TENGs at temperatures below 503 K. However, it appears that for the sliding mode TENG at 413, 443, and 473 K, Q_{SC} decays rapidly during initial measurements, while the contact–separation mode TENG showed slower charge decay at the beginning followed by a sharper decline. Both operational modes of TENGs

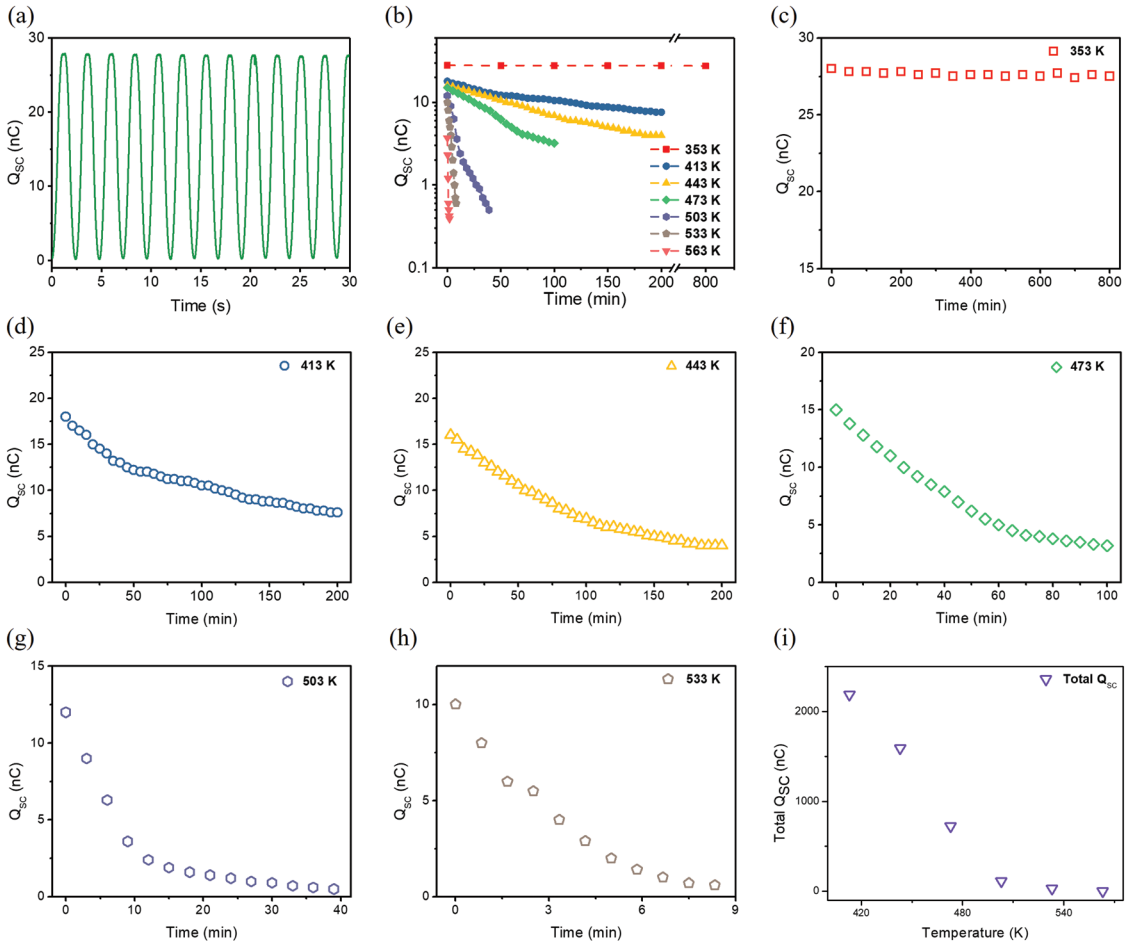

Figure 2. Performance of the Ti–SiO_2 sliding mode TENG at different temperatures with induced charge of −28 nC. a) The total transferred changes at room temperature. b–i) Q_{SC} evolution with time under different high temperatures: (c) 353 K, d) 413 K, (e) 443 K, (f) 473 K, (g) 503 K, (h) 533 K. (i) Integration of the decay curves from (d) to (h), showing total Q_{SC} measured under different high temperatures ranging from 413 to 563 K.

show a rapid initial decline of surface charge leading to exponential decay at 503 K and above. By integrating over these curves to determine the total amount of surface charge collected over the measurement time, an apparent decline in this value is also observed in Figure 2i as temperature increases, which may be attributed to the thermionic emission of electrons from the surface due to thermal energy fluctuations overpowering the charge generation and transfer effect of the TENG. This plot excludes the integration over the measurement taken at 353 K, not only because the time scale is much larger than that of the higher temperature measurements, but also because it is meant to show the evolution of the charge in states being directly affected by temperature effects. The relaxation time for charges also appears to shorten considerably as temperature increases, perhaps due to the greater mobility of charges from the surface until an equilibrium state is reached. The more immediate, sharper initial decay of Q_{SC} in precharged sliding mode TENGs below 503 K may result from less efficient generation of charges when precharged above a certain charge density due to saturation. Owing to the higher maximum displacement required for sliding to achieve the same maximum open-circuit voltage $V_{OC,max}$, the performance of a sliding TENG tends to be less efficient than that of a contact–separation TENG.[18] However, this does not explain the overall longer time scales for sliding mode charges to dissipate compared to contact–separation mode charges. To investigate this, measurement and analysis of charge retention without the influence of precharging is performed.

In order to evaluate the sliding mode Ti–SiO2 TENGs performance without initially induced charges on the surface, the charge on the triboelectric surfaces were eliminated using the process depicted in **Figure 3**a, in which ethanol and 2-propanol were applied and dried with Ar gas for three cycles per test. The measured Q_{SC} would then only be associated to the charges generated and transferred by the sliding mode TENG. In this case, even at the highest tested temperature of 563 K, the TENG was still able to increase the amount of transferred charges for a period of time through continual sliding interactions. The magnitude of transferred charges per TENG cycle decreases across the board as testing temperatures increase, as well as the period of time that charges can build up (Figure 3b). This collective plot differs greatly from the precharged measurements from Figure 2b, due to the lack of precharged electrons on SiO_2 in order to demonstrate the sliding TENGs capability

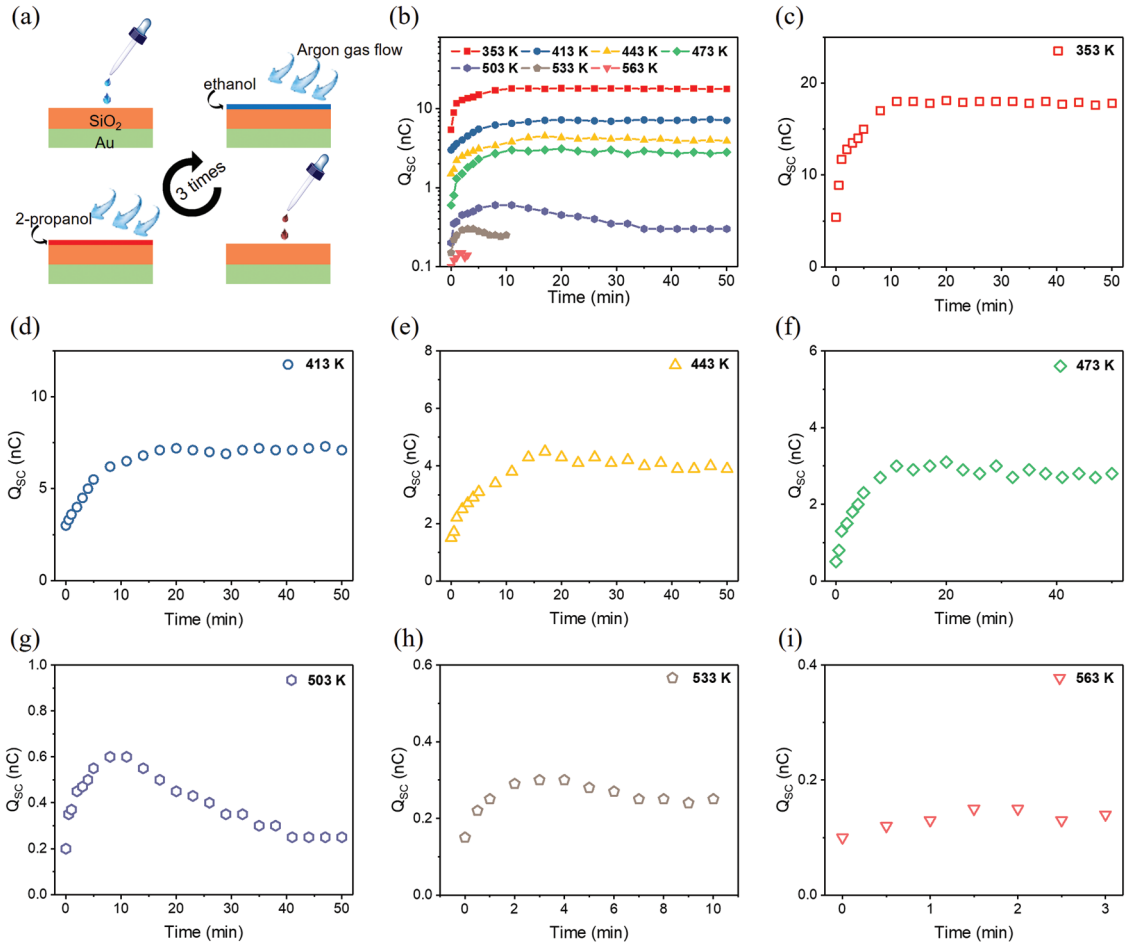

Figure 3. Performance of the Ti–SiO_2 sliding mode TENG at different temperatures without induced charges. a) Process of eliminating the initial charges on the surface of SiO_2. b–i) Q_{SC} evolution with time under different high temperatures: (c) 353 K, (d) 413 K, (e) 443 K, (f) 473 K, (g) 503 K, (h) 533 K. (i) 563 K.

to charge surfaces even in very high temperatures. There is a shorter time scale required for the uncharged TENG measurements to reach a similar plateau Q_{SC} value as the precharged TENGs, aside from the 353 K measurement, since the TENG was able to retain all precharged electrons for that condition. The individual plots of Q_{SC} over time at increasingly higher temperatures (Figure 3c–h) show a decay pattern emerging at and above 503 K following an elevated period from charge production by the TENG. The decrease is associated with thermionic emission overtaking the charge-generating mechanism of the TENG and causing a decrease in transferred Q_{SC}. The onset of this decay occurs earlier as temperature increases above 503 K, since electrons experience thermal energy fluctuations more rapidly at higher temperatures. The decay does not quite appear to be exponential or consistent in some of these cases aside from 503 K (Figure 3g), as the overall Q_{SC} measured at these temperatures is so close to 0 nC the change is less noticeable. At temperatures below 503 K, the repeated sliding displacement and reunion of triboelectric surfaces was sufficient to prevent dissipation of transferred charges from the exposed surfaces. The operation of the sliding mode TENG without initial charging was able to maintain TENG-produced charges more successfully at certain temperatures at which the precharged contact–separation mode TENG was unable to (e.g., 413, 443, 473 K).[15] Thereby, we suggest that the sliding mode is more efficient at generating and retaining charges at high temperatures when emission of electrons is at play, despite the lower figure of merits of sliding mode TENGs. These findings are supported by a recent systematic study on the maximal power of TENGs, which found that sliding-triggered TENGs are less limited by air breakdown and have higher energy density than contact–separation TENGs.[27] With the comparisons drawn from these results, TENGs for commercial applications have even more room to grow.

When contrasting the initially PU foam-charged samples with those that had charges eliminated from their surface, the Q_{SC} of initially discharged TENGs whose operation was able to overcome the influence of thermionic emission would plateau around the value that the initially charged TENGs would reach after exponential decay occurred. Therefore, this value appears to be a saturation point tied to its corresponding temperature and a Q_{SC} above or below it will eventually plateau at said value, although it takes longer for an oversaturated surface to lose charge and reach this point than an undersaturated

surface to gain charge to this point. This is likely due to the efficient charge retention capability of the sliding mode Ti–SiO_2 TENG. Notably, the precharged sliding mode TENG had higher Q_{SC} output only at 353 K (Figure S3, Supporting Information), but produced the same amount of Q_{SC} per operation cycle at higher temperatures and was not able to overcome thermionic emission like the uncharged sliding TENG. Additionally, the precharged and uncharged sliding mode measurements at 353 K do not reach the same plateau point as the other measurements do. This is due to the precharged SiO_2 measurement in Figure 2c retaining all of the precharged electrons since thermionic emission has not occurred significantly at this temperature and the charges likely do not exceed the air breakdown limit. Therefore, they remain on the precharged SiO_2 surface throughout the TENG operation, which by itself can only generate what is measured in Figure 3c. If the precharged and uncharged sliding mode measurements were performed at temperatures lower than 353 K such as room temperature, the trends would likely match the data from the 353 K measurements. Whether precharged or uncharged initially, the closeness of surfaces sliding together more continuously has greater potential to prevent discharge or emission at high temperatures than when in an intermittently separated motion. Even so, discharge from dielectric surfaces is possible during the sliding process if voids or gaps of at least 1 µm are present,[28] so protection of surface charges from thermionic emission may not be maximized by changing operational mode alone.

2.2. Electron Transfer Corroborated by the Sliding Mode Ti–SiO_2 TENG

In order to further implicate thermionic emission of surface charges and provide further evidence for electrons as the charge identity in charge transfer, the Q_{SC} data from the initially charged Ti–SiO_2 TENG tests at temperatures above 443 K were set against the simulated exponential decay model identified previously for contact–separation TENGs.[15] Unlike the fairly good fit of 443 K (**Figure 4**a), the residual charges at 473 (Figure 4b) and 533 K (Figure 4d) follow a less rapid fast-slow decay than that simulated, with a slower initial decline and a less severe transition into the slower decay portion. For 503 (Figure 4c) and 563 K (Figure 4e), the initial decline is faster and the transition is more immediate into the slow decay period compared to the simulated curve. As these discrepancies were also observed in the previous study, perhaps increasing volume of tests being averaged may match the data points to the exponential decay model more closely. Moreover, the plot of $\ln(J/A_0/T)$ against $1/T$ in Figure 4f fits their linear relationship quite well, showing a strong correlation of surface charge data with the thermionic emission equation.[15] The adequate fit of the sliding mode TENG data to simulated thermionic emission curves serves to provide further evidence of electron-dominated charge transfer in CE.

When comparing our sliding mode data to previous contact–separation mode findings,[15] we can associate the increased time scale required for near-complete emission of surface electrons as well as the ability to retain and generate charges at higher temperatures due to the protective nature of the sliding mode TENG against discharge. As this operational mode allows for longer periods of overlapping triboelectric surfaces, the effects of thermionic emission are dampened up until a certain temperature. Also, although the Q_{SC} rapidly decayed at higher test temperatures for the contact–separation mode Ti–SiO_2 TENGs, the sliding mode TENG was capable of generating even a small amount of transferred charge (0.05 nC) before decay took over at the highest tested temperature (563 K).

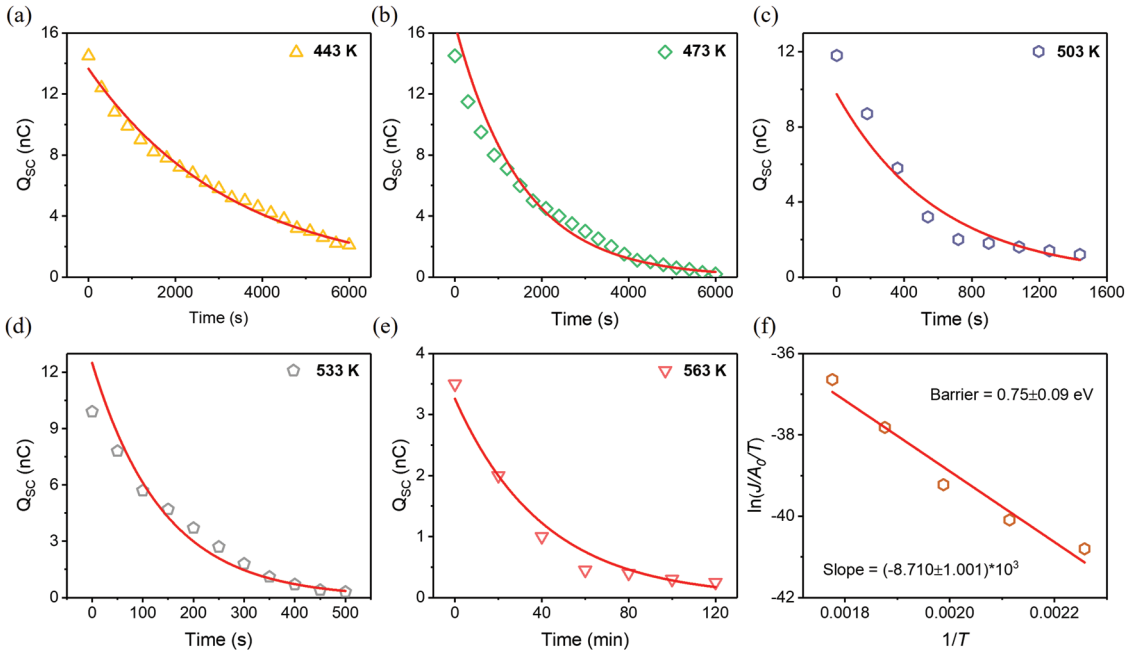

Figure 4. The measured (data points) and simulated curve based on electron thermionic emission model (solid) Q_{SC} as a function of the time at various temperatures. a) 443 K, b) 473 K, c) 503 K, d) 533 K. e) 563 K. f) Plots of $\ln(J/A_0/T)$ against $1/T$.

In addition to Q_{SC}, surface charge density is also a satisfactory variable in investigating temperature effects on TENGs, and a recent study using and tapping mode AFM has found that triboelectric charge decay follows the thermionic emission model at nanoscale.[29] It would be of great interest to continue this line of research by using contact scanning mode AFM to mirror a sliding mode TENG.

3. Modified Electron Cloud–Potential Well Model for Sliding Mode CE at High Temperatures

Based on the mechanism of CE from the newfound data on high temperature sliding mode TENGs, a modified electron cloud–potential well model is proposed for CE resulting from the sliding operational mode at elevated temperatures (**Figure 5**). This model may be applied to general triboelectric pair materials under these conditions in sliding contact, including metal–dielectric and dielectric–dielectric pairs. Since electrons in a general dielectrics do not have individual energy levels like in metals and semiconductors,[30] the electron clouds and potential well model are presented as universal characteristics that all materials possess. Even in the presence of factors such as surface impurities and chemical/atomic structure of materials that complicate dielectric CE studies, this model should apply, although these additional factors will also have an impact, especially certain material characteristics at high temperatures. This model also offers an explanation for the prolonged charge retention and improved charge generation efficiency of sliding mode TENGs at high temperatures.

First off, the model shows two materials completely displaced from each other and their electron clouds filled with electrons that are localized to specific atomic or molecular orbitals (Figure 5a). In this state, material A is negatively charged from the initially induced charges that were implemented in the first set of tests, and no electron transfer is occurring since it has not contacted material B yet. The difference in charge between the two materials is not as apparent without the precharging unless the materials are far apart on the triboelectric series. At high temperatures, the negatively precharged material A exhibits thermionic emission of surface charges at this state of noncontact, represented by the red directional arrows. Material B is not indicated to have any significant thermionic emission since its electrons are at an equilibrium state, and it would take a much more extreme temperature to induce emission of electrons from material B. When the two materials are

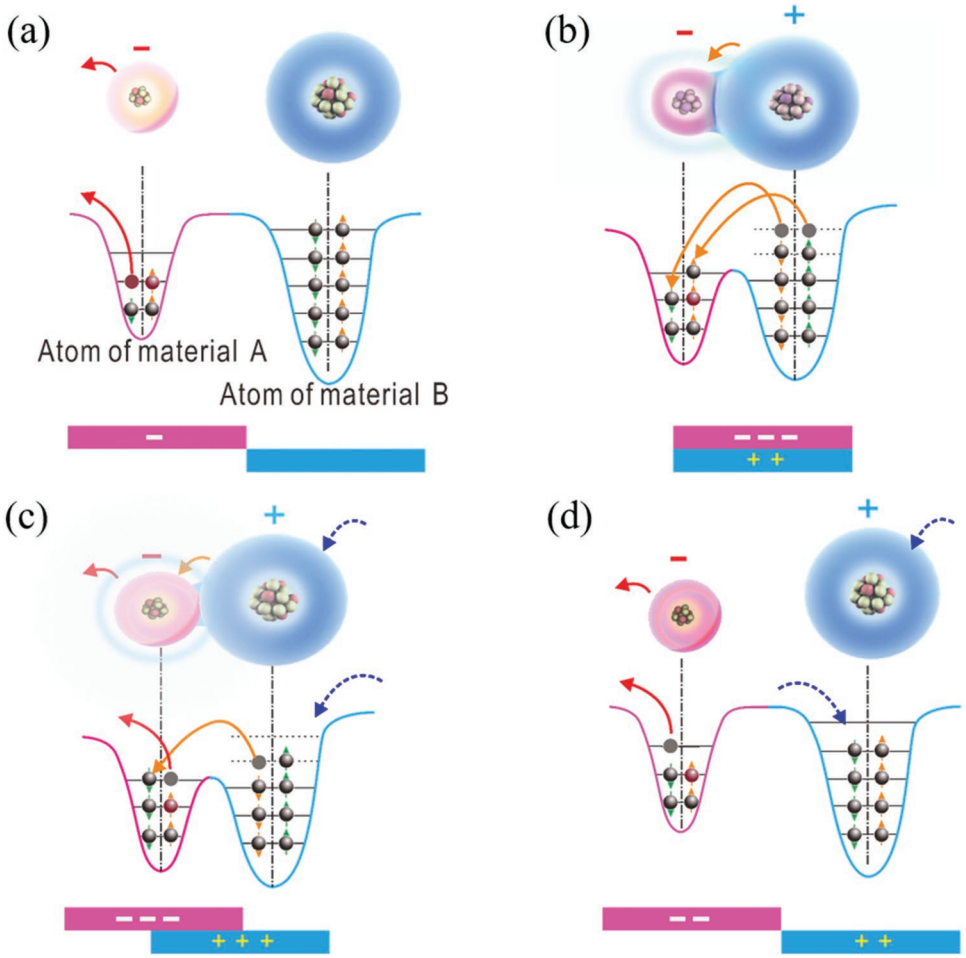

Figure 5. An electron cloud–potential well model proposed for explaining CE (this si called Wang transition) and charge transfer and release between two materials in the sliding-mode TENG. a) Initial state. b) Contact state. c) Semiseparated state. d) Separated state.

in contact when sliding against one another (Figure 5b), the electrons may be transferred from material B to material A due to CE and the development of equal and opposite charges on both surfaces when the materials are fully contacted. In this state, electron thermionic emission from the surface of SiO_2 is theoretically not present since the two surfaces are in such close contact. The electron clouds in Figure 5b demonstrate the overlap of clouds that occurs when two surfaces are closer than the interatomic distance at equilibrium, where long range attractive forces are equal to short range repulsive forces so charge transfer may occur.[31] These overlap areas or contact points occur from the presence of an externally applied force, and they occur on a very small fraction of the area between two surfaces in contact. However, they still play an instrumental role in facilitating CE, as has been validated by previous AFM studies.[29,31,32] The transfer of electrons, represented by the orange arrows, corresponds with the respective charge of each material surface in this state.

When the two materials begin to be displaced from the fully contacting state as they slide against each other along a single plane (Figure 5c), both the thermionic emission from the exposed areas of the negative material A and charge transfer from the areas in contact are affecting the measured total charges in sliding mode TENG. The emission of electrons from material A is represented by the red arrowheads, charge transfer by the orange arrowheads, and the flow of electrons through the circuit to balance the positive material B by the blue arrowheads. When the two materials are completely displaced once more (Figure 5d), the residual charges on the surface of the negative material A dissipate more rapidly due to thermionic emission and the lack of shielding by material B. As the displaced area increases to be greater than the contact area, thermionic emission overtakes the charge generation effects of the sliding mode TENG. The emitted electrons are represented by the red arrowheads and the electrons traveling through the circuit due to the potential imbalance between the materials is demonstrated by the blue arrowheads. The behavior of nearly all metal–dielectric and dielectric–dielectric pairs in sliding mode operation at high temperature may be modeled using this electron cloud–potential well model based on the rate of electron thermionic emission, the charge transfer rate of CE, the changing rate of the contacted area of between the two materials. Once the contacted area is dominant, the CE between the two materials is the major contributor. While the contact area is smaller than the displaced area, the thermionic emission of the exposed surfaces is the major contributor.

4. Conclusions

In summary, we compared the trends of thermionic emission of electrons between a sliding mode and previously tested contact–separation mode Ti–SiO_2 TENGs at elevated temperatures. The sliding mode TENG exhibited a sharper initial decline in charges below 503 K when precharged with PU to ≈28 nC compared to the precharged contact–separation mode TENG. However, in an initially uncharged state, the sliding mode TENG was able to overcome the influence of thermionic emission even at the highest tested temperature to increase transferred charges for a period before succumbing to exponential decay, which was not observed in the contact–separation TENG tests. This and the observation that the time scale for charge dissipation is much longer in sliding mode TENGs, both precharged and uncharged, are perhaps due to the prolonged shielding of discharge from the material surfaces in a continuous sliding motion as compared to an intermittent contact–separation motion. Lastly, the combined phenomena of CE charge transfer, and thermionic emission and the change in surface contacting areas are incorporated into a model of sliding mode CE between metal–dielectric and dielectric–dielectric pairs at high temperatures.

In general, high temperature operation of TENGs is not widely studied due to the degradation of many materials in such conditions under constant changing contact, as well as the low power output of materials at that state. Understanding the fundamentals behind charge behavior and optimized design are both important in furthering this front. Clearly, as CE may occur in a variety of different operational modes and is highly variable, controlled experiments with TENGs that have tailored designs and flexible material choices are valuable in studying the mechanisms of CE and developing its universal model. A rolling mode TENG study at high temperatures would be useful in analyzing the differences in charge generation and retention between the sliding and rolling modes, which have already had many comparative studies in terms of tribology. As sliding TENGs have been determined to be the best mode for both efficient high temperature operation and maximal power density, more investigations on other existing modes are necessary to form a solid knowledge foundation for the commercialization of TENGs.

5. Experimental Section

Fabrication of the TENG: SiO_2 sheets (99%) of 0.3175 cm thickness were purchased from Technical Glass Products. Their thermal conductivity was 1.4 W m K^{-1} (293 K) and their dielectric constant was 3.75 (299 K, 1 MHz). Ti foil (99.7%) with a thickness of 0.0032 cm was purchased from Sigma-Aldrich Co., LLC. PU foam was purchased from McMaster-Carr. Polytetrafluoroethylene film and Kapton film were purchased from American Durafilm. The Ti foil and SiO_2 were used as triboelectric pair materials. A Au coating on the back of the SiO_2 with a thickness of 300 nm was deposited as an electrode by using a Denton Explorer E-beam Evaporator. The deposition rate of Au coating was 0.2 nm s^{-1}. After Au deposition, the SiO_2 was annealed at 673 K for 4 h in air. The Au-coated SiO_2 was clamped to an insulating and high-temperature-resistant ceramic plate attached to the steel bar connecting to the motor. The Ti foil was clamped against a second ceramic plate attached to a stationary heat-resistant steel platform. Ni wires were clipped behind the SiO_2 sheet positioned in contact with the Au electrodes and behind the Ti foil acting as its own electrode.

Measurement of the TENG: A computer programmed linear motor was secured on top of a heating cabinet (Barnstead/Thermolyne 6000 furnace), which provides a desired temperature with an accuracy of ±5 K. The heating rate of the cabinet was about 7.5 K min^{-1}. In order to protect the motor from high temperatures, a long steel rod was implemented through the open hole in the heating cabinet to separate the active surfaces from the linear motor. A cooling fan was positioned adjacent to the setup to keep it from overheating. The environmental relative humidity was less than 30%, as measured by a Shaw Superdew 3 hygrometer. During TENG performance measurement, the linear motor was effective in accurately controlling the position and speed of

mechanical stimulation, and the heating cabinet maintained the desired temperature. The effective area of the Ti–SiO_2 TENG was 10 cm^2. The short-circuit transfer charge Q_{SC}, open-circuit voltage V_{OC}, and short-circuit current I_{SC} of the TENGs were measured by a Keithley 6514 electrometer and collected by LabView software. Precharged tests were performed after charging ≈28 nC to the surface of SiO_2 using PU foam, and uncharged tests were performed after discharging the surface to nearly 0 nC by washing the triboelectric surfaces with ethanol and 2-propanol three times each and drying with Ar gas after each wash.

Supporting Information

Supporting Information is available from the Wiley Online Library or from the author.

Acknowledgements

The authors are thankful for the support from the Hightower Chair Foundation at the Georgia Institute of Technology.

Conflict of Interest

The authors declare no conflict of interest.

Keywords

contact electrification, nanogenerators, thermionic emission

Received: November 12, 2019
Revised: December 14, 2019
Published online:

[1] a) W. R. Harper, *Contact and Frictional Electrification*, Oxford University Press, New York **1967**; b) G. S. P. Castle, *J. Electrost.* **1997**, *40–41*, 13; c) A. G. Bailey, *J. Electrost.* **2001**, *51–52*, 82.

[2] a) J. Lowell, *J. Phys. D: Appl. Phys.* **1975**, *8*, 53; b) W. R. Harper, G. P. Thomson, *Proc. R. Soc. London, Ser. A* **1951**, *205*, 83; c) D. K. Davies, *J. Phys. D: Appl. Phys.* **1969**, *2*, 1533.

[3] a) D. J. Lacks, R. Mohan Sankaran, *J. Phys. D: Appl. Phys.* **2011**, *44*, 453001; b) E. Németh, V. Albrecht, G. Schubert, F. Simon, *J. Electrost.* **2003**, *58*, 3.

[4] a) A. M. Cowley, S. M. Sze, *J. Appl. Phys.* **1965**, *36*, 3212; b) T. Mizutani, Y. Takai, T. Osawa, M. Ieda, *J. Phys. D: Appl. Phys.* **1976**, *9*, 2253; c) J. Lowell, *J. Phys. D: Appl. Phys.* **1977**, *10*, 65; d) Y. Zhang, T. Shao, *J. Phys. D: Appl. Phys.* **2013**, *46*, 235304; e) X. Shen, A. E. Wang, R. M. Sankaran, D. J. Lacks, *J. Electrost.* **2016**, *82*, 11; f) C.-y. Liu, A. J. Bard, *Chem. Phys. Lett.* **2009**, *480*, 145.

[5] a) Z. L. Wang, *Science* **2006**, *312*, 242; b) Z. Wang, G. Zhu, Y. Yang, S. Wang, C. Pan, *Mater. Today* **2012**, *15*, 532; c) C. Wu, A. C. Wang, W. Ding, H. Guo, Z. L. Wang, *Adv. Energy Mater.* **2019**, *9*, 1802906; d) F.-R. Fan, Z.-Q. Tian, Z. Lin Wang, *Nano Energy* **2012**, *1*, 328; e) Z. Wen, Q. Shen, X. Sun, *Nano-Micro Lett.* **2017**, *9*, 45; f) Z. L. Wang, *Mater. Today* **2017**, *20*, 74.

[6] a) J. Chen, J. Yang, Z. Li, X. Fan, Y. Zi, Q. Jing, H. Guo, Z. Wen, K. C. Pradel, S. Niu, Z. L. Wang, *ACS Nano* **2015**, *9*, 3324; b) Z. L. Wang, T. Jiang, L. Xu, *Nano Energy* **2017**, *39*, 9.

[7] Z. Zhao, X. Pu, C. Du, L. Li, C. Jiang, W. Hu, Z. L. Wang, *ACS Nano* **2016**, *10*, 1780.

[8] a) Y. Xie, S. Wang, S. Niu, L. Lin, Q. Jing, J. Yang, Z. Wu, Z. L. Wang, *Adv. Mater.* **2014**, *26*, 6599; b) F. Yi, X. Wang, S. Niu, S. Li, Y. Yin, K. Dai, G. Zhang, L. Lin, Z. Wen, H. Guo, J. Wang, M.-H. Yeh, Y. Zi, Q. Liao, Z. You, Y. Zhang, Z. L. Wang, *Sci. Adv.* **2016**, *2*, e1501624; c) F. Yi, J. Wang, X. Wang, S. Niu, S. Li, Q. Liao, Y. Xu, Z. You, Y. Zhang, Z. L. Wang, *ACS Nano* **2016**, *10*, 6519.

[9] a) X.-S. Zhang, M.-D. Han, R.-X. Wang, B. Meng, F.-Y. Zhu, X.-M. Sun, W. Hu, W. Wang, Z.-H. Li, H.-X. Zhang, *Nano Energy* **2014**, *4*, 123; b) Y. Yu, X. Wang, *Extreme Mech. Lett.* **2016**, *9*, 514; c) J. Wang, C. Wu, Y. Dai, Z. Zhao, A. Wang, T. Zhang, Z. L. Wang, *Nat. Commun.* **2017**, *8*, 88; d) L. Xu, T. Z. Bu, X. D. Yang, C. Zhang, Z. L. Wang, *Nano Energy* **2018**, *49*, 625; e) C. Zhang, W. Tang, C. Han, F. Fan, Z. L. Wang, *Adv. Mater.* **2014**, *26*, 3580.

[10] a) C. X. Lu, C. B. Han, G. Q. Gu, J. Chen, Z. W. Yang, T. Jiang, C. He, Z. L. Wang, *Adv. Eng. Mater.* **2017**, *19*, 1700275; b) J. Nie, Z. Wang, Z. Ren, S. Li, X. Chen, Z. Lin Wang, *Nat. Commun.* **2019**, *10*, 2264; c) Z. L. Wang, *Faraday Discuss.* **2014**, *176*, 447; d) Z. L. Wang, J. Chen, L. Lin, *Energy Environ. Sci.* **2015**, *8*, 2250; e) K. Xia, C. Du, Z. Zhu, R. Wang, H. Zhang, Z. Xu, *Appl. Mater. Today* **2018**, *13*, 190; f) Y. Yang, H. Zhang, J. Chen, Q. Jing, Y. S. Zhou, X. Wen, Z. L. Wang, *ACS Nano* **2013**, *7*, 7342.

[11] S. Niu, S. Wang, L. Lin, Y. Liu, Y. S. Zhou, Y. Hu, Z. L. Wang, *Energy Environ. Sci.* **2013**, *6*, 3576.

[12] S. Lin, L. Xu, L. Zhu, X. Chen, Z. L. Wang, *Adv. Mater.* **2019**, *31*, 1901418.

[13] a) A. Verdaguer, M. Cardellach, J. J. Segura, G. M. Sacha, J. Moser, M. Zdrojek, A. Bachtold, J. Fraxedas, *Appl. Phys. Lett.* **2009**, *94*, 233105; b) H. Sun, H. Chu, J. Wang, L. Ding, Y. Li, *Appl. Phys. Lett.* **2010**, *96*, 083112; c) S. Li, Y. Zhou, Y. Zi, G. Zhang, Z. L. Wang, *ACS Nano* **2016**, *10*, 2528.

[14] M. Willatzen, Z. Lin Wang, *Nano Energy* **2018**, *52*, 517.

[15] C. Xu, Y. Zi, A. C. Wang, H. Zou, Y. Dai, X. He, P. Wang, Y. C. Wang, P. Feng, D. Li, *Adv. Mater.* **2018**, *30*, 1706790.

[16] E. L. Murphy, R. H. Good, *Phys. Rev.* **1956**, *102*, 1464.

[17] C. Xu, A. C. Wang, H. Zou, B. Zhang, C. Zhang, Y. Zi, L. Pan, P. Wang, P. Feng, Z. Lin, *Adv. Mater.* **2018**, *30*, 1803968.

[18] Y. Zi, S. Niu, J. Wang, Z. Wen, W. Tang, Z. L. Wang, *Nat. Commun.* **2015**, *6*, 8376.

[19] K. Nicholson, U. O. Newcastle, P. Ireland, E. Wanless, G. Jameson, *Design and Construction of a Laboratory Scale Cyclone Tribocharger*, Engineers Australia, Barton, Canberra, Australia, September-October **2008**, pp. 1130–1136.

[20] P. M. Ireland, *Powder Technol.* **2010**, *198*, 199.

[21] J. Hu, P. Gu, Q. Zhou, C. Liang, D. Liu, X. Chen, *Powder Technol.* **2018**, *340*, 484.

[22] T. Tokeshi, K. i. Hiratsuka, A. Sasaki, S. Uchiyama, C. Kajdas, *Tribol. Trans.* **2009**, *52*, 759.

[23] Z. Rymuza, *Arch. Civil Mech. Eng.* **2007**, *7*, 177.

[24] a) B.-B. Jia, T.-S. Li, X.-J. Liu, P.-H. Cong, *Wear* **2007**, *262*, 1353; b) N. S. Eiss, B. P. McCann, *Tribol. Trans.* **1993**, *36*, 686; c) J. Rojsatean, P. Larpsuriyakul, N. Prakymoramas, D. Thanomjitr, S. Kaewket, T. Singsom, D. Srinun, *Tribol. Int.* **2017**, *109*, 229.

[25] K. Sayfidinov, S. D. Cezan, B. Baytekin, H. T. Baytekin, *Sci. Adv.* **2018**, *4*, eaau3808.

[26] P. M. Ireland, *J. Phys. D: Appl. Phys.* **2008**, *41*, 025305.

[27] J. Fu, X. Xia, G. Xu, X. Li, Y. Zi, *ACS Nano* **2019**, *13*, 13257.

[28] A. Wåhlin, G. Bäckström, *J. Appl. Phys.* **1974**, *45*, 2058.

[29] S. Lin, L. Xu, C. Xu, X. Chen, A. C. Wang, B. Zhang, P. Lin, Y. Yang, H. Zhao, Z. L. Wang, *Adv. Mater.* **2019**, *31*, 1808197.

[30] a) J. F. Hughes, *Phys. Bull.* **1987**, *38*, 424; b) F. A. Vick, *Br. J. Appl. Phys.* **1953**, *4*, S1.

[31] Z. L. Wang, A. C. Wang, *Mater. Today* **2019**, *30*, 34.

[32] Y. S. Zhou, Y. Liu, G. Zhu, Z.-H. Lin, C. Pan, Q. Jing, Z. L. Wang, *Nano Lett.* **2013**, *13*, 2771.